Biofilm characterisation of the maize rot-causing pathogen, *Fusarium verticillioides*

Chizné Peremore, Cairin van 't Hof, Cebo-LeNkosi Nkosi, Kadima Tshiyoyo, Francinah M. Ratsoma, Wisely Kola, Samkelo Malgas, Quentin Santana, Brenda Wingfield, Emma T. Steenkamp & Thabiso E. Motaung

View supplementary material

Published online: 09 Jun 2025.

Submit your article to this journal

View related articles

View Crossmark data

Biofilm characterisation of the maize rot-causing pathogen, *Fusarium verticillioides*

Chizné Peremore[a,b], Cairin van 't Hof[a]*, Cebo-LeNkosi Nkosi[a]*, Kadima Tshiyoyo[a], Francinah M. Ratsoma[a,b], Wisely Kola[a,b], Samkelo Malgas[a], Quentin Santana[b,c], Brenda Wingfield[a,b], Emma T. Steenkamp[a,b] and Thabiso E. Motaung[a,b] (ID)

[a]Department of Biochemistry, Genetics and Microbiology, University of Pretoria, Hatfield, Pretoria, South Africa; [b]Forestry and Agricultural Biotechnology Institute, University of Pretoria, Hatfield, Pretoria, South Africa; [c]Biotechnology Platform, Agricultural Research Council, Pretoria, South Africa

ABSTRACT

Biofilm formation was investigated in a maize rot-causing pathogen, *Fusarium verticillioides*. This work revealed that *in vitro* cultures produce structured, adherent communities with a dense extracellular matrix (ECM) surrounding hyphae that makes up the biomass of a matured biofilm. Pellicle containing exopolysaccharide had a hydrodynamic diameter of 4.19 nm and a low viscosity (0.022 dl/g). The exopolysaccharide was composed of amino sugars and unordered, facilitating stability through complexation with the anionic eDNA. Biofilm formation varied over different pH and temperature values, emphasising its role in promoting adaption, survival, and persistence in *F. verticillioides*, potentially contributing to its pathogenicity in maize. Collectively, the results provide valuable insights into biofilm structure and stress resistance in this fungus, and will serve as a foundation for future studies incorporating in planta infection systems.

Introduction

After rice and wheat, maize (*Zea mays*) is the third most abundant grain crop, feeding millions of people, particularly in Sub-Saharan Africa. However, its growth yield is threatened by *Fusarium verticillioides*, which systemically colonises leaves, stems, roots, and kernels. The fungus can therefore induce serious damage that often manifests in *Fusarium* ear and stalk rot (Oren et al. 2003; Gai et al. 2018). These diseases have food safety and security implications due to mycotoxin contamination that is associated with the fungus. Primarily, *F. verticillioides* secretes the mycotoxin, fumonisin B_1, which contaminates symptomatic and asymptomatic maize kernels and stored grains (Munkvold and Desjardins 1997). The toxicity of this compound is due to the inhibition of ceramide synthase and subsequent toxic intracellular accumulation of sphingosine and other sphingoid bases (Marin et al. 2013), ultimately imposing detrimental health effects on consumer populations (Wild and Gong 2010).

Indeed, studies from around the globe, including some from Africa, Asia, and Latin America, paint a disconcerting picture of how the prevalence of mycotoxins leads to a variety of human pathologies, including oesophageal and liver cancer in adults who consumed contaminated maize (Wild and Gong 2010).

The mechanisms by which *F. verticillioides* invades maize have been outlined (Oren et al. 2003; Gai et al. 2018), providing important clues on the circumstances leading to infection symptoms and the precise anatomical locations of the maize plant that would probably harbour mycotoxins. The production of mycotoxins by *Fusarium verticillioides* has often been given far more attention than the production of virulence factors in many studies on mycotoxigenic fungi. The current study posits that the development of biofilms is somehow closely related to the accumulation of mycotoxins in fungi. A key indicator of this connection is the biofilm's 3D structure and biomass, which isencased in extracellular polymeric substances (EPS). The

encapsulation of a group of adherent fungal cells by the protective layer, called an extracellular matrix (ECM), gives rise to the biofilm. Together, the polysaccharides (such as mannans and β-glucans), proteins, lipids, and extracellular DNA that make up this matrix chemically offer protection and structural stability (Harding et al. 2009). This structural design gives rise to emergent characteristics that are only seen in the biofilm mode of microbial life, such as surface adhesion, spatial organisation, physical and social interactions, chemical heterogeneity, and greater tolerance to antimicrobials (Karygianni et al. 2020).

In the case of mycotoxigenic fungi, the biofilm EPS may exert a substantial effect on mycotoxin production; it may permit mycotoxins to stably accumulate and persist for longer periods as it glues the cells together, in the process creating pockets and channels through which mycotoxins can be concentrated and distributed within a biofilm, respectively. *Aspergillus fumigatus* biofilms, for instance, augment the production of gliotoxin, a sulphur-containing mycotoxin with immunosuppressive properties (Bruns et al. 2010). An interesting area of research will be determining the extent that components within a biofilm, including the EPS and its associated cell-free components such as the extracellular DNA (eDNA), influence mycotoxin production. Therefore, research on biofilms will provide a fresh perspective on mycotoxin synthesis in pathogenic fungi.

As biofilms present a cross-sectoral challenge, affecting a wide range of sectors including healthcare, built environment, food and agriculture (Cámara et al. 2022), the current lack of understanding of how filamentous fungal biofilms originate, and how they adapt to their microenvironments once developed, restrict our capacity to identify and counter their detrimental impacts. This is apparent in the clinical setting, where most clinical infections associated with medical instruments, including indwelling devices colonised by biofilms, are difficult to treat due to antifungal resistance of these cell community structures (Donlan 2001; Lindsay and Von Holy 2006; Bryers 2008). Ships and underwater surfaces are examples of colonised surfaces, and their treatment is difficult due to concurrent and intolerable environmental impacts on non-target species (Callow and Callow 2011; Bixler and Bhushan 2012). The same type of challenges might apply to agriculture, where some of the essential and most used tools and machinery are contaminated with harmful fungal biofilms that are challenging to remove (Harding et al. 2009; Ramage et al. 2011). When employed across many fields, farming equipment colonised by biofilms

has the potential to contaminate unaffected fields with biofilm-derived propagules that may have acquired novel traits within a biofilm, including resistance to fungicides (Costa-Orlandi et al. 2014).

Compared to microbial biofilms in medical settings, the research of biofilms in plant pathogenic fungi is still in its infancy. Although several fungi, such as *Magnaporthe oryzae, Botrytis cinerea*, and *Fusarium spp*., have demonstrated the capacity to create biofilm-like communities, little is known about their precise structure, control, or function in plant infection. Somewhat formal descriptions of biofilms in plant fungal pathogens have started to emerge (Motaung et al. 2020), with the latest being provided for the *Phaeomoniella chlamydospore* (Karácsony et al. 2024), *F. graminearum* (Shay et al. 2022), and *F. circinatum* (Ratsoma et al. 2024). Under *in vitro* settings, *F. graminearum* has been demonstrated to produce structured biofilms composed of linked hyphal networks that are contained in an extracellular matrix rich in eDNA and polysaccharides (Shay et al. 2022). According to Karácsony et al. (2024), *P. chlamydospora* creates biofilms that obstruct grapevine xylem arteries, causing water flow disruption and exacerbating esca disease symptoms. Additionally, by strengthening the pathogen's resistance to antifungal agents, these biofilms make infections more enduring and challenging to manage. A good example is the pine pitch canker fungus, *F. circinatum*, which develops strong biofilms composed of extracellular matrix and hyphal bundles that increase its resilience to heat, antifungals, and DNase (Ratsoma et al. 2024). This may promote its persistence in the field when harsh conditions are present, potentially facilitating adaptability and pathogenicity. These results imply that one of the main virulence strategies of plant-pathogenic fungi is the production of biofilms.

However, to date, the role of biofilm formation in many disease-causing plant fungi, including key biofilm components such as eDNA and EPS, has not been elucidated. The current study sought to elucidate how the morphology of surface-associated *F. verticillioides* might be included in current biofilm descriptions. Our research will contribute to a better understanding of how filamentous plant fungal pathogens coordinate survival by forming a community structure.

Materials and methods

Fungal strains and maintenance

Strains of *F. verticillioides* were obtained from a culture collection in the Forestry and Agricultural

Biotechnology Institute (FABI), University of Pretoria, following isolation from maize samples taken from fields in the Eastern Cape province of South Africa. Two strains (CMWF 1196 and CMWF 1197) were screened for their ability to form biofilms in this study. The strains were plated on $1/4$ strength PDA (Potato Dextrose Agar; 1% (w/v) PDA powder and 1.2% (w/v) Difco agar) and allowed to grow for two weeks at room temperature. The matured cultures were then used to develop biofilms in liquid media as described below.

Screening for biofilm formation

Rapid screening of biofilm formation was performed for all fungal isolates by cutting a block of agar (5 mm × 5 mm) from the sporulating culture and inoculating it into 15 ml of three different growth media in 50 ml Falcon tubes; $1/4$ Potato Dextrose Broth (PDB), Roswell Park Memorial Institute-1,640 broth (RPMI) and Sabouraud Dextrose Broth (SDB). After mixing, the inoculated solution was poured into petri dishes (100 mm × 15 mm) and incubated at 25 and 30 °C for 24–72 hrs. The cultures were visually analysed every 24 hrs for biofilm formation, which is a hyphal assemblage that appears in the form of a cloudy and thin slime material, and photographed with an Epson Perfection V700 Photo scanner (Harding et al. 2009; Mowat et al. 2009).

Biofilm formation for the remaining experiments was conducted using a cell counting method. To do this, the inoculum for counting cells was prepared by adding 2 ml of 1× phosphate-buffered saline (PBS, 137 mM NaCl, 2.7 mM KCl, 10 mM Na_2HPO_4, and 1.8 mM KH_2PO_4) onto the sporulating culture of $F.$ $verticillioides$ that was grown on $1/4$ PDA for seven days. The plate was swirled to allow spores to be released into the PBS and then counted using a haemocytometer placed under a Zeiss Axioskop 2 plus Light Microscope. To distinguish between dead and living cells in the fungal culture, 40 μl of cell culture suspension was mixed with 40 μl of 0.4% (w/v) Trypan Blue solution (Sigma-Aldrich) into an Eppendorf tube. The concentration of the harvested conidia was adjusted to 1×10^5 conidia/ml in $1/4$ PDB. A volume of 200 μl of the adjusted harvested conidia culture was added to 48 wells plates (Corning® Costar® TC- Treated Multiple Well Plates from Sigma-Aldrich) or chamber slides (Lab- Tek® Chamber SlideTM System, 8 Well Permanox® Slide) and incubated for seven days at 25 °C (Cavalheiro and Teixeira 2018). The culture was then analysed using different microscopic techniques as explained later.

Analyses of biofilm-like structures

To better describe the biofilms formed by $F.$ $verticillioides$, colony and cell morphology were first analysed on plates containing liquid media (PDB), where the former was examined visually every 24 hrs for 7 days. Following the visual screening, the spores were cultured in $1/4$ PDB with agitation (180 rpm) (Shake-O-Mat, LABOTEC) and stationary conditions for 72 hrs in chamber slides, harvested and then analysed under a light microscope (Zeiss Axioskop 2 plus Light Microscope (LM)). A scanning electron microscope (SEM) was used to study the ultrastructure of biofilms formed as previously described, in chamber slides or 48-well plates with glass coverslips (LASEC SA). Sample preparation for SEM was performed according to Harding et al. (Harding et al. 2010). Samples were examined with Zeiss Ultra PLUS FEG SEM Confocal Laser Scanning Microscopy (CLSM). This was used to analyse $F.$ $verticillioides$ biofilms by forming biofilms in chamber slides at different time points (24 hrs and 7 days) and staining them for 30 mins in a dark room with 100 μl of FUN-1, which fluorescent viability probe for fungi. Biofilms were then visualised using Zeiss LM 880 CLSM with excitation wavelength at 488 nm and emission at 650 nm.

Analysis of biofilm-derived cells

This study considered whether biofilm-derived cells are different from planktonic cells in $F.$ $verticillioides$. To do this, biofilms of $F.$ $verticillioides$ were formed as previously mentioned. After 7 days of incubation, cells were extracted from the biofilm by scraping and briefly agitated (30 s) to loosen the cells from the EPS matrix. This suspension was filtered through Mira cloth (Sigma-Aldrich) to separate the cells from the EPS material. In parallel, $F.$ $verticillioides$ planktonic cells were scraped from the sporulating cultures on $1/4$ PDA and added to PBS. The cells were then counted and adjusted to the desired concentration (1×10^5 spores/ml). A volume of 10 μl was aliquoted onto $1/4$ PDA and incubated at 25 °C for 7 days. The agar plates were then examined to study differences in growth and colony morphology, with three sections of each biofilm-derived and planktonic cells examined with Zeiss Ultra PLUS FEG SEM.

Quantification of biomass, EPS and metabolic activity

Biofilm biomass was determined by measuring the production of EPS and metabolic activity. To measure

the biofilm biomass, crystal violet was used as it is known to be a good indicator of the amount of cellular biomass (Cruz et al. 2018). Biomass was then quantified according to a previously described method (Mello et al. 2016). Biofilms in 96 well plates (Corning® Costar® TC- Treated Multiple Well Plates (Sigma-Aldrich) were fixed for 15 min in 200 µl of 99% methanol. The supernatant was then removed, and the biofilm that was attached in microtiter plates was air-dried for 5 min before adding 200 µl of 0.3% crystal violet solution (stock solution diluted in PBS; Sigma-Aldrich) to each well. The stained biofilms in microtiter plates were then incubated for 20 min at room temperature before being rinsed twice with PBS to remove excess dye. The biomass in each well was then decolourised with 200 µl of 99% ethanol for 5 min. A volume of 100 µl of this solution was then transferred to a new 96-well plate and the absorbance was measured at 590 nm using a microplate reader (SpectraMax® Paradigm® Multi-Mode Detection Platform).

The extracellular matrix was quantified according to the method described by Mello et al. (Mello et al. 2016). Biofilms in 96 well plates (Corning® Costar® TC- Treated Multiple Well Plates (Sigma-Aldrich) were stained for 5 min at room temperature with 20 µl of 0.1% safranin (stock solution diluted in PBS: Sigma-Aldrich). After that, the stained biofilms were rinsed with PBS till the supernatants became transparent. With 200 µl of 99% ethanol, the extracellular matrix was decolourised. A volume of 10 µl of the supernatant was transferred to a fresh 96-well plate, and the absorbance at 530 nm was measured using a microplate reader as previously reported. To measure the metabolic activity of the biofilm, biofilms were formed in 96-well plates as before and incubated at 25 °C. Once biofilms had been formed, their metabolic activity was then quantified using a colourimetric assay, XTT (sodium 3´- [1- (phenylaminocarbonyl)- 3,4- tetrazolium]-bis (4- methoxy6-nitro) benzene sulfonic acid hydrate) (Sigma-Aldrich), according to the manufacturer's recommended specifications. The activity of fungal mitochondrial dehydrogenase converts XTT tetrazolium salt to XTT formazan, resulting in a colour change that can be measured using the microplate reader as previously described, with the absorbance from each well measured at 492 nm.

The impact of abiotic conditions on biofilm growth

The impact of abiotic conditions on biofilm production by *F. verticillioides* was assessed at different pH values (2, 3, 4, 5, 6, 7, 8) and temperatures (10, 15, 20, 25 and 35 °C) in ¼ PDB. The pH was adjusted using HCl and NaOH. To conduct these experiments, standardised spore suspensions were inoculated as previously described, and biofilms were allowed to develop under the aforementioned abiotic conditions for 7 days. Quantification of biomass, EPS, and metabolic activity was then performed using the microplate reader as previously described. Following this, EPS and biomass were determined, with EPS expressed per biomass (i.e. EPS/Biomass) and metabolic activity percentages calculated to compare the response of biofilms under the different physical factors.

Effect of DNase treatment on biofilm formation

The eDNA release was measured using a microplate-based fluorescence assay using a DNA-binding dye (SYBR® Green I), as previously described by Rajendran et al. (2014). For this study, biofilms were cultivated in ¼ PDB for 7 days at 25 °C before being scraped from the plates using sterile cell scrapers and rinsed with PBS. The EPS was extracted from the disaggregated biofilm using 0.2 M EDTA. Following this, the samples were centrifuged at $10,000 \times g$ for 30 min, the EDTA supernatant was collected and filtered through a 0.45 µm syringe filter (Millipore). SYBR® Green I (Invitrogen), whose binding results in fluorescence that is directly proportional to DNA content, was applied at a 1:4 ratio to biofilm supernatants in a black well microtiter plate (Costar3603; Corning). The levels of eDNA were then quantified using a fluorescence plate reader (SpectraMax® Paradigm® Multi-Mode Detection Platform) at 485 and 525 nm, respectively. The concentration of eDNA in the sample was quantified using the DNA standard curve as previously described (Leggate et al. 2006).

The role of eDNA in *F. verticillioides* biofilm formation was investigated by depletion of eDNA within the biofilm using the hydrolytic enzyme (Rajendran et al. 2013), and DNase I from bovine pancreas (Sigma-Aldrich). The DNase I was prepared in 0.15 M NaCl supplemented with 5 mM MgCl₂. To assess the effect of DNase I on biofilm formation, biofilms were formed in ¼ PDB as described above and were incubated with DNase I at the concentrations of 0.25, 1, and 2 mg/ml, and incubated at 25 °C for 72 hrs and 7 days. Untreated controls were included for direct comparison. After each treatment, the biofilms were washed in PBS, and their metabolic activity, biomass, and EPS were quantified as mentioned previously.

EPS extraction of *Fusarium verticilloides* biofilm and composition analysis

Biofilm were developed in 2 l roller bottles containing 1 l of PDB inoculated with 2×10^6 cells/ml and incubated at room temperature for 7 days (Cavalheiro and Teixeira 2018). Post incubation, the PDB was discarded and the biofilm scraped into flasks containing 10 ml of 0.2 M EDTA to extract the EPS. The flasks were shaken for 3 hrs at 100 rpm the mixture dispensed into 50 ml Falcon tubes and centrifuged at 1,000 rpm for 30 min to recover the EPS. The supernatant was collected and placed into 66 mm petri-dishes and freeze-dried for 2 days, resulting in dried EPS, which was used for downstream analysis (Melo et al. 2022).

Protein content determination

The Bradford assay was employed to detect protein in the exopolysaccharide, as outlined previously, with bovine serum albumin (BSA) serving as a standard (Bradford 1976). Spectrophotometric measurements were conducted at 595 nm under room temperature, and protein concentration was estimated in terms of BSA equivalents per dry mass of the exopolysaccharide.

Phenolic content determination

The Folin-Coicalteu assay was employed to detect phenolics in the exopolysaccharide, as outlined previously, with gallic acid serving as a standard (Malgas et al. 2016). Spectrophotometric measurements were conducted immediately after the heating step at 40 °C, and the phenolic concentration was expressed as gallic acid equivalents per dry mass of the exopolysaccharide.

Total sugar content determination

The monosaccharide composition of the exopolysaccharide was determined after hydrolysis of 10 mg dry powder with 1 ml of 2 M trifluoroacetic acid (TFA) in a dry digital bath (Eins Sci, Johannesburg, South Africa) for 2 hrs at 120 °C. The residual TFA was evaporated from the sample using nitrogen gas. The sample was resuspended in 1 ml of deionised water for sugar analysis. The sulphuric acid-UV assay was used to estimate the total sugar content of the exopolysaccharide, using N-acetyl-glucosamine as a suitable standard. The method was developed and optimised using a previously described method (Albalasmeh et al. 2013). Spectrophotometric measurements at 290 nm were made at room temperature, and the total sugar was estimated and expressed as total sugar per dry mass of the exopolysaccharide.

UV spectroscopic determination of the degree of acetylation (DA)

Ultraviolet (UV) spectroscopy was employed according to a previously reported method whereby 25 mg of the exopolysaccharide was dissolved in 5 ml of 85% phosphoric acid at 60 °C for 40 min. One millilitre of the resulting solution was diluted to 100 ml with distilled water and incubated at 60 °C for 2 hrs before measurements. The determination of the degree of N-acetylation was carried out by using the UV value at 203 nm after calibration with monomer mixtures of glucose and N-acetyl glucosamine prepared in 0.85% phosphoric acid at concentrations of 0, 10, 20, 30, 40, 50 and 100 μg/ml (Liu et al. 2006; Wu and Zivanovic 2008).

Sulphate content determination

The sulphate content of the *F. verticillioides* exopolysaccharide was determined using the gelatine-barium method developed as described previously (Torres et al. 2021). Spectrophotometric measurements were conducted at room temperature and sulphate ion concentration was estimated in terms of Na_2SO_4 equivalents. Conducting the barium-chloride assay on both non- and hydrolysed exopolysaccharides allowed for the determination and discrimination between organic and inorganic sulphates contained in the sample.

Exopolysaccharide physical and structural analysis

Functional group analysis by FTIR

Exopolysaccharide functional group composition was investigated by FTIR using a Perkin Elmer Frontier spectrophotometer, equipped with a universal ATR diamond crystal sampling accessory (Waltham, United States). About 16 scans were collected over the $4,000 - 650 \text{ cm}^{-1}$ spectral range. Automatic baseline correction and normalisation of the spectra were conducted with Spectrum One software (Perkin Elmer). The degree of acetylation (DA) is the share of nitrogen sites occupied by acetyl groups (each nitrogen atom can react with one acetyl group). The DA of the exopolysaccharide was determined using the absorbance ratios of the amide II-band to the CH-stretching band as described previously (Beil et al. 2012).

Glycosidic linkage analysis by NMR

The sugar sequence and types of glycosidic linkages constituting the exopolysaccharide were analysed by ^{1}H and ^{13}C nuclear magnetic resonance (NMR) spectroscopy using a Bruker Avance III 400 MHz

spectrometer with a BBI probe (Bruker, Karlsruhe, Germany). For NMR analysis, the exopolysaccharide was suspended in D_2O (99.96%) (Merck, Darmstadt, Germany) and the spectra were recorded at ambient temperature. The spectra were processed and analysed using TopSpin NMR software (Bruker, Karlsruhe, Germany). For structural elucidation of the exopolysaccharide, the NMR chemical shifts obtained from ^{1}H and ^{13}C spectra were used for input to the CASPER webserver (Furevi et al. 2022; Dorst and Widmalm 2023).

Rheological and viscosity-average molecular mass analysis

To determine the intrinsic viscosity and viscosity-average molecular weight (Mv) of the *F. verticillioides* exopolysaccharide, solutions were prepared by dissolving the polysaccharide at 0.1–20 mg/ml in a 50 mM NaCl solution. The intrinsic viscosity ($[\eta]$) of the exopolysaccharide was determined by the average efflux time of each sample measured at 25 °C using a semi-micro viscometer (size: 50) (CANNON Instrument Company, State College, United States). First, the specific viscosity (η_{sp}) of the exopolysaccharide, which is calculated from the increment in viscosity due to the polymer, was calculated using Equation (1):

$$\eta_{sp} = \frac{t_a - t_0}{t_0} \qquad (1)$$

where t_a is the efflux time of the solution and t_0 is the efflux time of the solvent. The intrinsic viscosity ($[\eta]$) is defined as specific viscosity extrapolated to an exopolysaccharide concentration (C) of zero as follows (Equation 2):

$$[\eta] = \left(\frac{\eta_{sp}}{C} \right)_{C \to 0} \qquad (2)$$

where C is in g/ml. The viscosity-average molecular weight (Mv) of the exopolysaccharide was calculated using the Mark-Houwink equation (Equation 3). The *K* (0.00016) and α (0.79) are constants for a given solute-solvent system and temperature.

$$[\eta] = KMv^{\alpha} \qquad (3)$$

Particle size analysis by DLS

The particle size of the exopolysaccharide was determined by dynamic light scattering (DLS) using a Genizer Dual-Light Nano Particle Sizer (Irvine, United States), with a standard green laser (30 mW and 570 nm). Scattering was analysed at 25 °C using a 4 ml quartz cuvette, with samples diluted to 0.1–10 mg/ml concentrations in 50 mM NaCl. For all the samples, the mean value of three measurements was taken at a photon counting rate of around 40 for a green laser with a delay time of 5 μsec. The LPSA software was used to obtain the hydrodynamic diameter using the cumulant analysis with a repeatability of 5% and size distribution (polydispersity index, PdI) of the exopolysaccharide.

Structural conformation determination by Congo red assay

The conformational structure of the exopolysaccharide in an aqueous solution was determined by characterising the Congo red-polysaccharide complex as described previously (Guo et al. 2021). Solutions of the exopolysaccharide (1 mg/ml), 80 μM Congo red and NaOH with different concentrations (0, 0.1, 0.2, 0.3, 0.4 and 0.5 M) were prepared. Meanwhile, water instead of the polysaccharide solution was used as the control. After being kept for 10 min at room temperature, λmax was measured at a wavelength range of 400 to 600 nm using a plate reader.

Water solubility and conductivity determination

The solubility of the exopolysaccharide was determined by dissolving 1 g of the polysaccharide in 100 ml of dH_2O with constant stirring for 5 min at 25 °C. Prepared suspensions were then centrifuged for 5 min at 12 000 ×g. The supernatant was removed, while the non-dispersible pellet of the exopolysaccharide was dried at 40 °C overnight. The tubes were weighed, and the mass of the dispersible fraction was determined. To determine the conductivity, a 1% (w/v) exopolysaccharide solution was prepared in dH_2O. The conductivity of the exopolysaccharide solution was determined using an XS Tester PC5 Tester (Carpi MO, Italy). The reference temperature for the experiment was kept at 25 °C, and the results were expressed in μS/cm.

Statistical analysis

All experiments were performed in duplicate, in two independent experimental sets. The data were expressed as mean ± standard deviation (SD). The results were evaluated using the GraphPad Prism 9 computer program. A *p*-value of 0.05 or below was deemed statistically significant in all analyses (ns = $p > 0.05$; *= $p \leq 0.05$; **= $p \leq 0.01$; *** =$p \leq 0.001$; ****= $p \leq 0.0001$). In addition, a one-way ANOVA was used to determine significant differences between samples.

Results

Colony morphology of *in vitro* biofilm-like structures

The ability of *F. verticillioides* to form biofilm-like structures was observed in both strains examined in this study (Figure 1). Then, using visual inspection of liquid cultures, colonies emerging from a biofilm culture were observed in PDB, SDB and RMPI, incubated at 25 °C from 24 hrs to 7 days (data not shown). The biofilm is normally distinguished from planktonic cells by the occurrence of dense, highly hydrated clusters of cells enmeshed in a gelatinous matrix (Hurlow and Bowler 2009; Metcalf and Bowler 2013; Coraça-Huber et al. 2020). Indeed, *F. verticillioides* biofilm-like colonies displayed a dense, thin, and cloudy material (Figure 1). Based on these morphological traits, the biofilm-like formations will be referred to as simply biofilms from this point on.

Fusarium verticillioides biofilm development

Two *F. verticillioides* isolates, CMW 1196 and CMW 1197, were screened for their capacity to produce biofilms *in vitro*. Preliminary analyses revealed that the isolates had comparable growth patterns, morphological traits, and biofilm-forming abilities (Figure 1). These isolated had been obtained from the same host and geographic area and since their performances were similar, only CMW 1196 was chosen for more thorough examination. Biofilms were formed consistently across all tested media types, demonstrating the fungus's inherent ability to develop structured communities under varied conditions. This approach ensured a clearer, more focused presentation of the most representative and robust findings.

It was anticipated that a biofilm would form most effectively under stationary conditions and that the shear stress from shaking would prevent the formation of the EPS matrix, a distinguishing feature of microbial biofilms. Therefore, the cells from *F. verticillioides* CMW 1196 were cultured under both shaking and stationary conditions. Following this, planktonic cells cultivated under shaking conditions did not typically clump together when observed under a light microscope (Figure 2A), while those cultivated under stationary conditions developed a community of cells resembling a biofilm (Figure 2B). When these cells were analysed under SEM, little to no EPS formation was visible around cells cultivated under shaking conditions (Figure 2C). However, cells that were cultivated without shaking formed visible EPS (Figure 2D), which was not surprising given that EPS has been observed often after growth under non-shaking conditions in biofilm investigation studies (Cavalheiro and Teixeira 2018).

Fusarium verticillioides biofilms and impact on cells therein

The development of a biofilm in *F. verticillioides* may influence the metabolic status of cells and, by extension, their phenotype (Ramage et al. 2012). Our observations were in agreement with this, as the spores at the dispersion stage (Figure 3C) appeared to be morphologically distinct from the normal microconidia spores initially used as the inoculum to initiate a biofilm (indicated in Figure 3A). Usually,
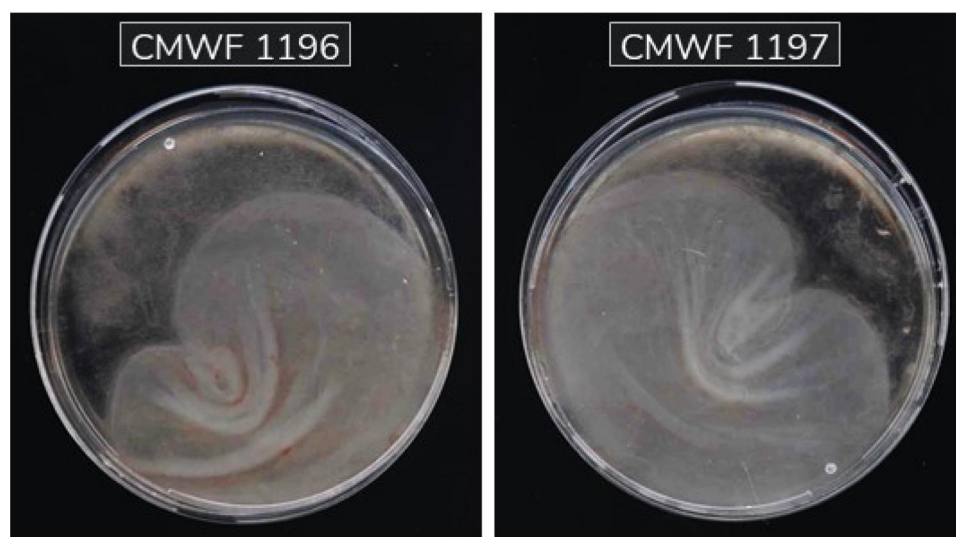

Figure 1. *Fusarium verticillioides* strains that formed biofilm-like cultures in Petri-dishes containing ¼ strength Potato Dextrose Broth. The strains were left to grow, without shaking, for 7 days at 25 °C.
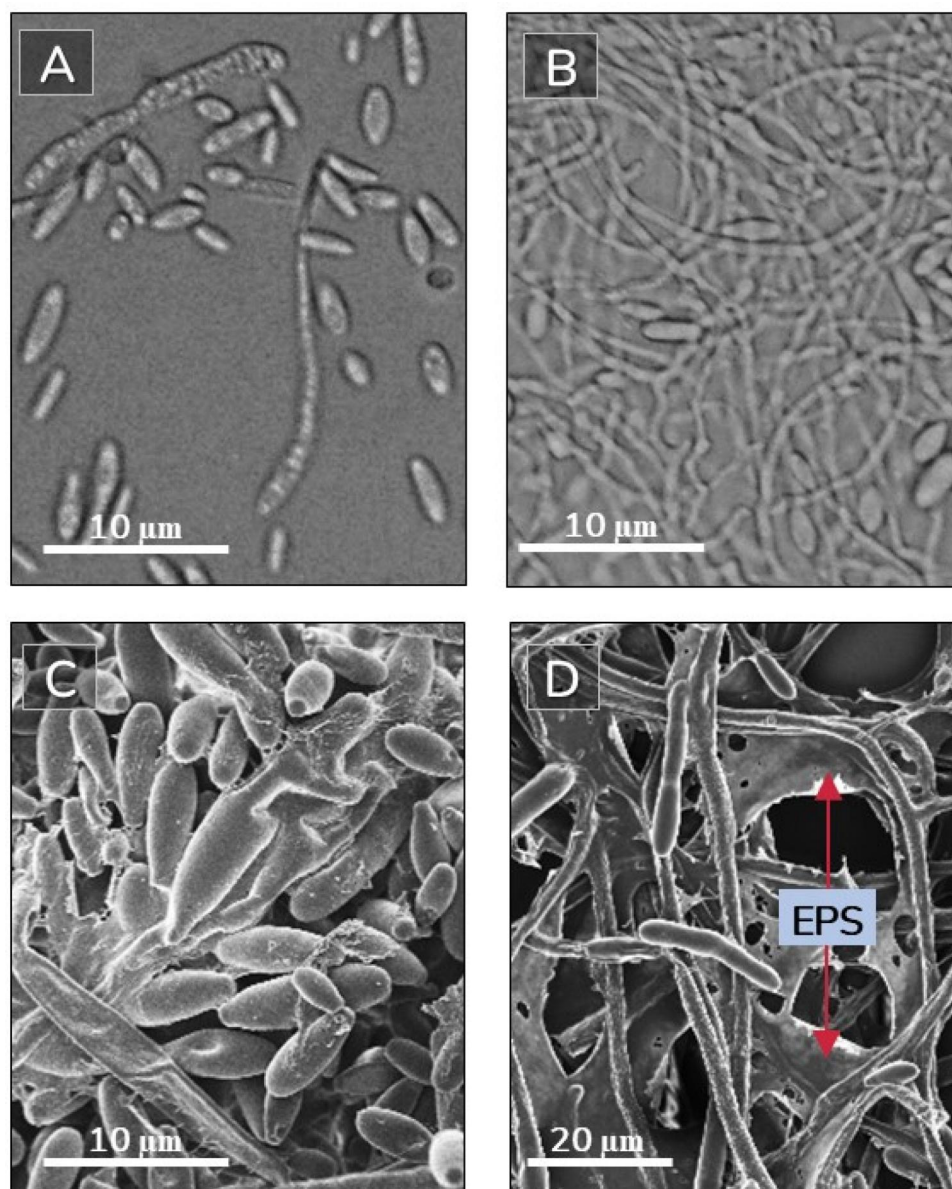
Figure 2. *Fusarium verticillioides* cultured for 7 days under shaking conditions (**A, C**), remained in the planktonic (free-living) state, and without shaking (**B, D**), formed biofilms with observable extracellular polymeric substances (EPS, indicated by red arrows in **D**).

microconidia of *F. verticillioides* are club- or elliptical-shaped or pointed at both ends (Figure 3A). However, the biofilm-derived spores were more globose/lemon-shaped and slightly larger than typical conidial cells (Figure 3C). Therefore, biofilm-derived cells, as indicated in Figure 3D, may influence phenotypic diversity in *F. verticillioides*. For instance, when these cells were harvested from a biofilm and plated on ¼ strength PDA, they displayed a colony morphology that differed from cells not derived from a biofilm, i.e. they formed a colony smaller than that of their planktonic counterpart (Figure 3). The physiological responses of cells within a biofilm are likely shaped by the dynamics of its ecosystem. However, the morphology of cells derived from a biofilm had

no apparent differences when compared to the morphology of planktonic cells (Supplementary Figure 2), suggesting that the differences between these cells might largely be in their response to environmental signals, as in the case with observations in Figure 3, as opposed to their morphology.

Biofilm biomass, metabolic activity and EPS production

The complexity of the biofilm is, for the most part, due to the release of EPS (Ramage et al. 2011). This means that the biofilm may possess the ability to affect the physiology of the cells within it by holding
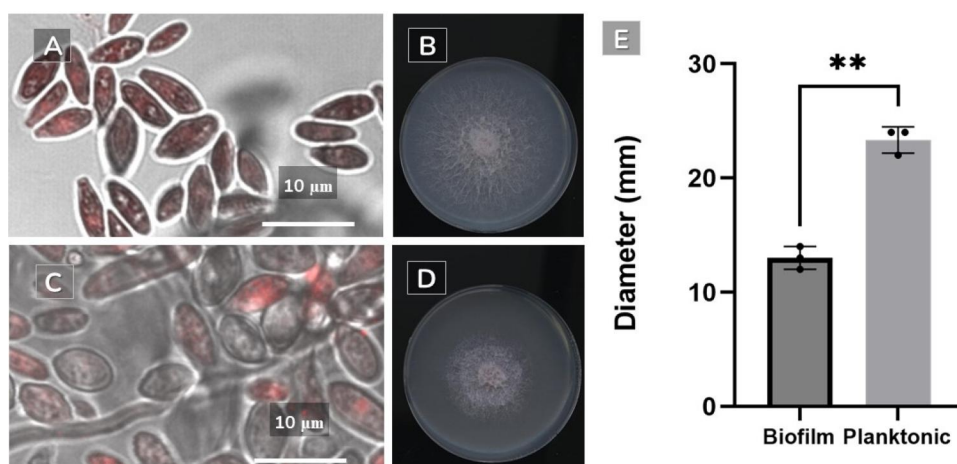
Figure 3. *Fusarium verticillioides*, colony and cell morphology analysis. The cells were stained with FUN-1 to determine biofilm development at **(A)** 24 hrs and **(C)** at 7 days. Biofilm-derived and planktonic cultured *F. verticillioides* in chamber slides for *F. verticillioides* cells from biofilm-derived**(B)** and planktonic **(D)** cultures established colonies on ¼ PDA. Colonies derived from biofilm cells of asexual cells that were formed were significantly smaller (** = $p \leq 0.01$) than those derived from planktonic cells **(E).** a The respective cells were all plated at the same concentrations and incubated under the same conditions. Each dot on the bar graphs represents an independent biological replicate. ns= $p > 0.05$; *= $p \leq 0.05$; **= $p \leq 0.01$; *** = $p \leq 0.001$; ****= $p \leq 0.0001$.

them in place, thus maintaining the biofilm's 3D structure while also optimising the exchange of nutrients and genetic material. As previously indicated, the results showed that, unlike cells cultured under shaking conditions (Figure 2A, C), the generation of a visible EPS occurs concurrently with the establishment of a mature biofilm (Figure 2B, D). To assess the amount of EPS produced during *F. verticillioides* biofilm formation and the contribution of metabolically active cells to the total biomass, colourimetric assays were used, namely crystal violet and XTT, to analyse the biomass and to evaluate the metabolic activity (cell viability) of the biofilm, respectively. In the case of the XTT reduction assay, the production of soluble coloured formazan salts by sessile cells is a direct reflection of cellular metabolic activity. According to the results, an increase in cell mass and EPS production (Figure 4) was accompanied by an increase in metabolic activity of the cells inside the biofilm (Figure 4); EPS/biomass increased significantly from 13% (3 days) to 45% (7 days) ($p = 0,002$), suggesting that as the biofilm matures more EPS is produced.

Biofilm formation in response to abiotic factors

Having shown that *F. verticillioides* asexual cells could develop into a biofilm, this study then investigated how the biofilm reacts to different environmental conditions, namely different temperature and pH conditions. As shown in Figure 5A, EPS/biomass was highest at pH 5, suggesting that *F. verticillioides* may
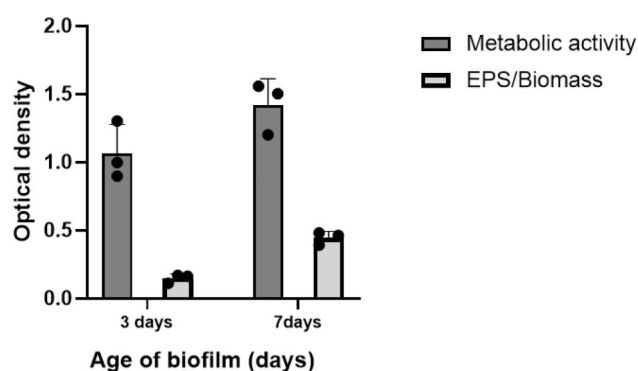

Figure 4. *Fusarium verticillioides* biofilm formation was assessed based on metabolic activity, evaluated by XTT reduction assay and biomass and extracellular polymeric substances (expressed as EPS/Biomass) evaluated using crystal violet (OD$_{590nm}$) and safranin (OD$_{530nm}$), respectively (p-value = 0.0013). An increase in cell mass and EPS production is observed. Each dot on the bar graphs represents an independent biological replicate. ns= $p > 0.05$; *= $p \leq 0.05$; **= $p \leq 0.01$; *** =$p \leq 0.001$; ****= $p \leq 0.0001$.

prefer pH 5 for biofilm formation. The media that was used in the initial experiments (¼ PDB) has a pH of around 5, and it was in this medium that all the stages of a biofilm were observed (Figure 2). The EPS and metabolic activity were essentially the same at acidic pH levels (i.e. 2, 3, and 4, below the optimal pH of 5), whereas at pH levels higher than the optimal (i.e. pH 6, 7, and 8), the EPS was produced at lower levels and plateaued at these levels. From the optimal pH (pH 5) point of view, *F. verticillioides* biofilms seem to produce significantly more EPS/ Biomass than at pH 6 and pH 8 ($p \leq 0.05$). However,

this biofilm had a significantly lower metabolic activity at the range of pH values tested distinct from pH 5 (2, 3, 4, 6, 7, and 8) ($p \leq 0.001$). This suggests that the biofilm response to pH is versatile, which could influence the adaptability of this pathogen to a range of field conditions.

Figure 5C and 5D depict the influence of temperature on the production of *F. verticillioides* biofilms.

The fungus displayed similar metabolic activities and formed robust biofilms at 20 and 25 °C with no significant differences. The fungus also formed biofilms at 10, 15 and 35 °C, but these were not as robust at 20 and 25 °C, and their cells had lower metabolic activity. Different temperatures do not seem to significantly affect the EPS/biomass yield except for 10 °C, where the biomass was undetectable.
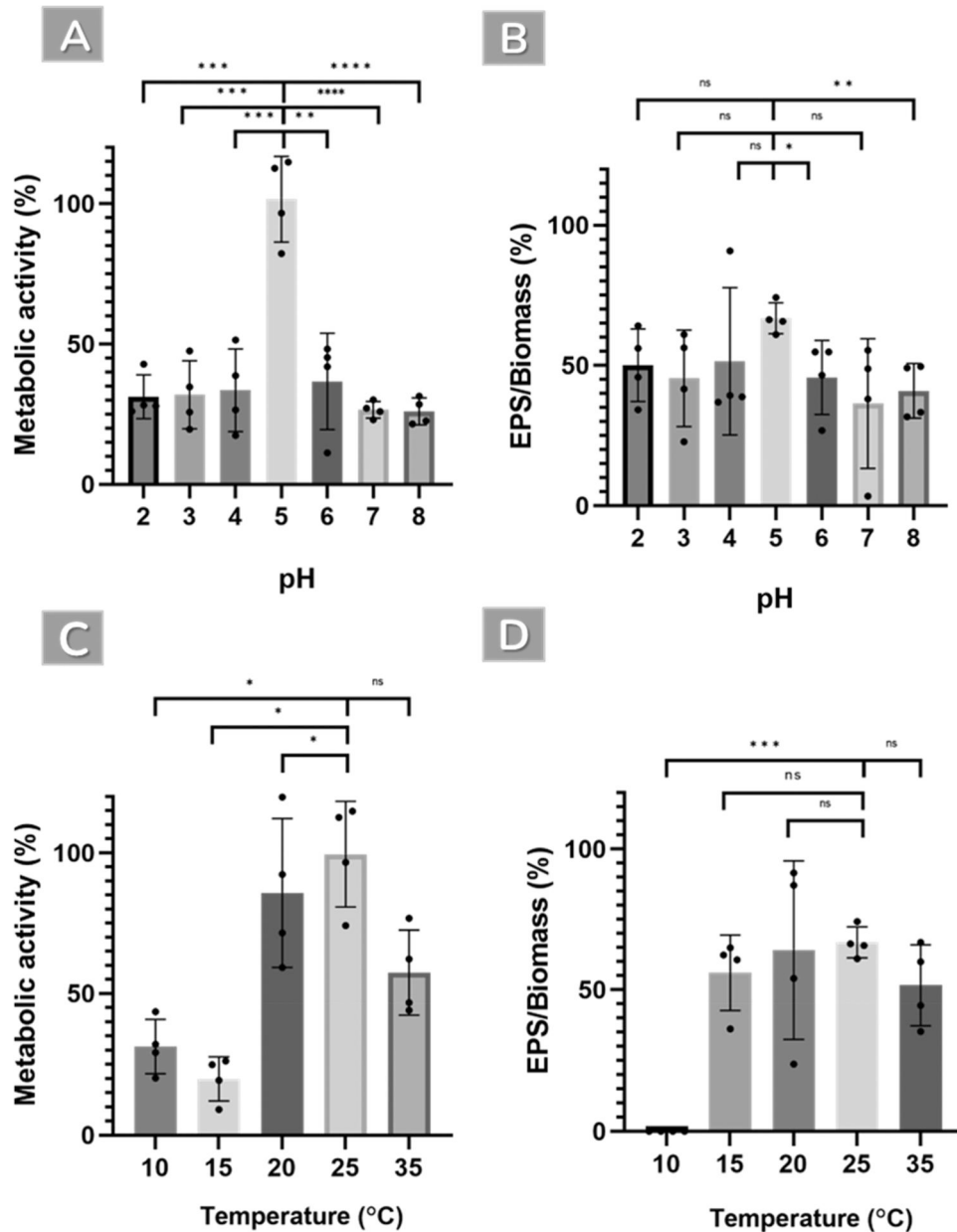

Figure 5. *Fusarium verticillioides* biofilm formation assessed at various pH and temperature conditions by measuring **(A, C)** metabolic activity (XTT reduction assay (OD$_{475nm}$; p value < 0.05) (expressed as metabolic activity percentage)), and **(B, D)** biomass and extracellular polymeric substances (expressed as EPS/Biomass percentage), evaluated using crystal violet (OD$_{590nm}$) and safranin (OD$_{530nm}$), respectively (p value < 0.05). This data shows that pH 5 permits better biofilm formation, and the biofilm response to pH is versatile, spanning a range of pH conditions. The optimum temperatures evaluated for metabolic activity were 20 and 25 °C. It also generated biofilms at 10, 15, and 35 °C, but these were less robust and had lower metabolic activity. Different temperatures do not appear to have a significant impact on the EPS/Biomass %, except for 10 °C, when the biomass could not be quantified. Each dot on the bar graphs represents an independent biological replicate. ns= $p > 0.05$; *= $p \leq 0.05$; **= $p \leq 0.01$; *** =$p \leq 0.001$; ****= $p \leq 0.0001$.
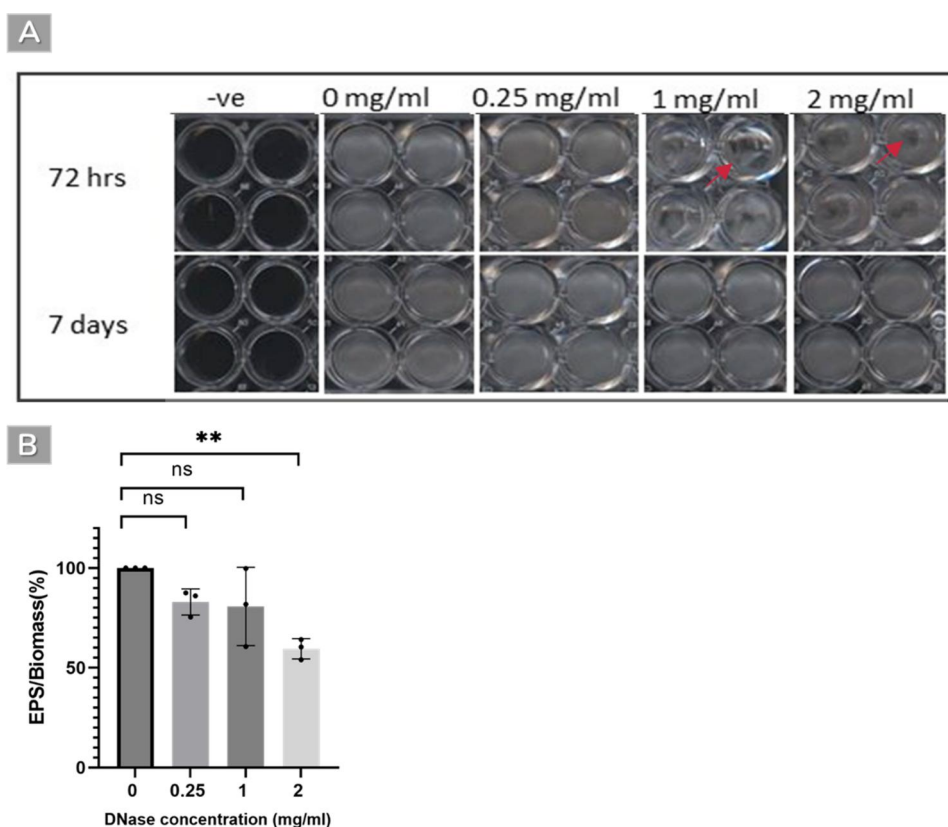
Figure 6. *Fusarium verticillioides* biofilm response to DNase treatment. The response of a 72-hr-old and 7-day-old biofilm to DNase at different concentrations (0.25, 1 and 2 mg/ml) **(A)**. The response of biofilms measured in biomass and extracellular polymeric substances (expressed as EPS/Biomass percentage) to DNase at different concentrations (0.25, 1 and 2 mg/ml) **(B)**. This data shows that DNase I caused the collapse of biofilm formation at the early stages of growth, i.e. at 72 hrs, and the structural integrity of the biofilm was found to be strongly influenced by DNase I in a concentration-dependent manner. Each dot on the bar graphs represents an independent biological replicate. ns= $p > 0.05$; *= $p \leq 0.05$; **= $p \leq 0.01$; ***= $p \leq 0.001$; ****= $p \leq 0.0001$.

The structural integrity role of eDNA in biofilms

The biofilm was treated with DNase I to elucidate the role of eDNA in maintaining the structure of the biofilm. The DNase abolished biofilm formation during the early stages of development, i.e. at 72 hrs (Figure 6A). Also, the structural integrity of the biofilm was revealed to be significantly impacted by the addition of DNase I in a concentration-dependent manner. Unfortunately, the EPS/biomass yield could not be determined during the early biofilm maturation phase (72 hrs) as the biofilm had no substantial formation integrity to perform the relevant assays. In comparison to the biofilm growth control at 7 days, the application of 0.25 and 1 mg/ml DNase I slightly reduced EPS/biomass formation by 17% ($p > 0.05$) while 2 mg/ml of DNase I significantly reduced it by 40% ($p = 0.0095$) (Figure 6B). Interestingly, while DNase I influenced the formation of EPS and biomass, it did not significantly affect the metabolic activity of the biofilm (data not shown). This suggests that eDNA plays a more crucial role in the structure of EPS in the biofilm of *F. verticillioides* rather than

Table 1. Composition analysis of the *Fusarium verticillioides* exopolysaccharide, where the constituents are represented as a percentage on a dry mass basis.

Total carbohydrate	Protein	Phenolics	Sulphate	Degree of esterification
93.8 ± 0.6	Nd	5.33 ± 0.01	Nd	3.4 ± 0.0

Where Nd = not detected.

in its cellular activity, a finding that has also been demonstrated in other fungal species (Martins et al. 2012; Rajendran et al. 2014).

Exopolysaccharide composition analysis

The general compositional analysis of the *F. verticillioides* exopolysaccharide was determined after freeze-drying, and the constituents of dry matter weight are reported (Table 1). Overall, the composition analysis showed that the exopolysaccharide was exclusively composed of carbohydrates, with a minor phenolic content (5.33% on a dry mass basis).
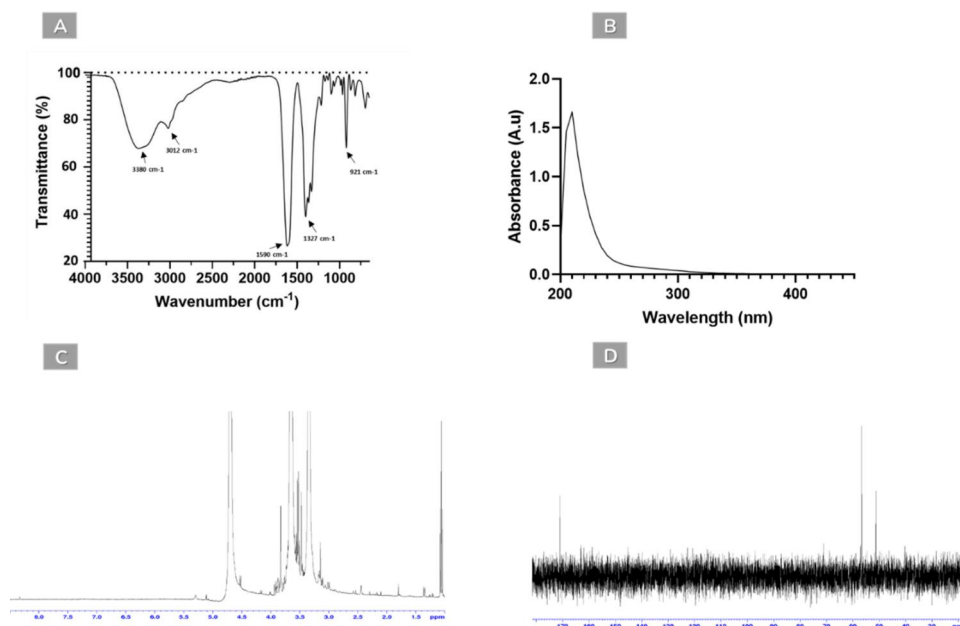
Figure 7. Structural characterization of the *F. verticillioides* exopolysaccharide. Determination of functional groups and electron transitions in chromophores constituting the *F. verticillioides* exopolysaccharide by **(A)** FTIR and **(B)** UV spectral scan. Determination of sugar sequence and types of glycosidic linkages constituting the *F. verticillioides* exopolysaccharide by **(C)** 1H NMR and **(D)** 13C NMR.

Exopolysaccharide functional group and structural monomeric units analysis

The FTIR spectrum of the exopolysaccharide displayed the characteristic absorption peaks of functional groups found in polysaccharides (Figure 7A). The exopolysaccharide displayed a large and strong absorption peak at $3,380 \, cm^{-1}$, attributed to the vibration of -OH stretching (Song et al. 2024). Its appearance at such a high frequency reflects increased hydrogen bonding interactions. The pronounced absorption peak at $3,012 \, cm^{-1}$ may be due to the stretching vibrations of C–H bonds in CH_3, CH_2 and CH (Kumirska et al. 2010). The peak displayed around $1,615 \, cm^{-1}$, with a shoulder at $1,590 \, cm^{-1}$, indicates the N-H bending vibration (amide II) (Prashanth et al. 2002), and the amide III band at $1,327 \, cm^{-1}$ was also detected (Beil et al. 2012). The splitting of the amide I band is due to the influence of hydrogen bonding or the presence of an enol form of the amide moiety, usually observed in α-chitinous polysaccharides. Finally, additional peaks were also observed at $1,395 \, cm^{-1}$ (asymmetrical deformation of CH_2) (Prashanth et al. 2002), $1,213 \, cm^{-1}$ (symmetric stretching vibration due to $S = O$ group, indicating the presence of sulfate group) (Daub et al. 2020) and $1,096 \, cm^{-1}$ (pyranose residue) (Song et al. 2024), and $921 \, cm^{-1}$ (C-H bending or C-O stretching vibrations) (Kumirska et al. 2010).

The UV-Vis absorption spectrum of the exopolysaccharide was also evaluated and displayed maximum absorption in the 205–215 nm wavelength range, which often results from $n − \sigma^*$ and $\pi − \pi^*$ transitions, which are found in many functional groups, such as amine, carboxyl, carbonyl and ester (Trabelsi et al. 2009), in polysaccharides (Figure 7B). Similarly, the amino sugar, acetyl-glucosamine, constituting chitinous polysaccharides, has been reported to absorb in the range of 190–220 nm (Wu and Zivanovic 2008). An absorption peak was not observed in the 260–280 nm region in the spectrum of the exopolysaccharide (Figure 7B). This indicated the absence of nucleic acids or protein content in the extracted polysaccharide, consistent with the composition analysis results shown in Table 1.

The anomeric configuration of the monosaccharides in the *F. verticillioides* exopolysaccharide was determined using ^{1}H (Figure 7C) and ^{13}C NMR (Figure 7D) spectroscopy. The faint doublet signal at δ1.34 and δ1.36 was attributed to H6 of the methyl group in 2-acetamido-2-deoxy-L-quinovose (Qui3N) (Shashkov et al. 1998, p. 247; Turska-Szewczuk et al. 2014, p. 1,298–1,316). The signals at δ3.14 and δ3.34 in ^{1}H NMR were assigned to H2 of a hexosamine (Pereira et al. 2015). Similarly, glucosamine (GlcN) residues in chitosan exhibit a signal at δ3.15 (Vårum et al. 1991). The signal at δ3.82 was attributed to H6 of the hexosamine Qui3N residue in the exopolysaccharide (Shashkov et al. 1998,

**Table 2.** 1H and ^{13}C NMR chemical shifts (ppm) of the *Fusarium verticillioides* exopolysaccharide.

Glycosyl linkage	H1/C1	H2/C2	H3/C3	H4/C4	H5/C5	H6/C6	Me_2	CO_2
→4) α-d-GalN	5.29	4.17	4.01	4.17	4.15	3.82	-	-
	-	51.1	-	-	-	-	-	-
→4) α-d-GalNAc	5.11	4.15	4.01	4.51 – 4.53	-	-	1.79	-
	-	51.1	-	-	-	-	-	171
α-d-QuiN	-	3.82	3.69	3.34	4.15	1.34 – 1.36	-	-
	-	56.3	-	-	-	-	-	-

Where - = corresponding signal not detected.

p. 247). Since there was no signal at $\delta 2.0 - 2.1$, it was concluded that most of the hexosamine residues in the exopolysaccharide did not contain an acetyl-H (Vårum et al. 1991; Furevi et al. 2022). Still, it is noteworthy that the exopolysaccharide exhibited a signal at $\delta 1.79$ that could be attributed to an acetyl-H. In the *F. verticillioides* exopolysaccharide spectra, a signal at $\delta 5.3$ could match with an α-anomer present at the reducing end of the polysaccharide and no β-anomer-associated signal ($\delta 4.7$) was present (Le Mauff et al. 2022). A faint amide proton signal at $\delta 8.33$ was observed in the ^{1}H NMR spectra of the exopolysaccharide.

The signals at $\delta 51.1$ and $\delta 56.3$ in the 13 C NMR spectrum were assigned to a carbon (C2) substituted by the amino group in monosaccharide residues. These signals were similar to the two nitrogen-bearing carbons at $\delta 49.15$ and $\delta 55.09$ (GalN C-2 and Qui3N C-3, respectively) reported for the lipopolysaccharide from *Aeromonas veronii* Strain Bs19, Serotype O16 (Turska-Szewczuk et al. 2014; Pereira et al. 2015). The ^{13}C NMR spectrum of the exopolysaccharide lacked a signal at $\delta 21 - 25$, where the -CH$_3$ of acetamide-containing hexosamine residues is displayed (Furevi et al. 2022), concurring with the ^{1}H NMR spectrum regarding a majority of the hexosamines in the exopolysaccharide structure containing an amine (-NH$_2$) at this position. Finally, the signal at $\delta 171$ was attributed to carbonyl carbon atoms, indicating some degree of acetylation in the exopolysaccharide (Vinogradov and Perry 2004).

Based on all the data obtained from FTIR and NMR, it was concluded that the biological repeating unit of the exopolysaccharide from *F. verticillioides* had the following structure (see Table 2 for linkage analysis):

$$\alpha\text{-d} - \text{QuiN} \; (1 \rightarrow 4) \; \alpha\text{-d} - \text{GalNAc} \; (1 \rightarrow 4) \; \alpha\text{-d} - \text{GalN}$$
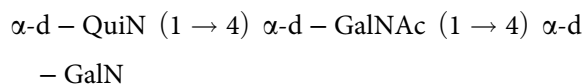
Physical properties determination of the *Fusarium verticillioides* exopolysaccharide

The physico-chemical properties of the *F. verticillioides* exopolysaccharide, such as its intrinsic viscosity, viscosity-average molecular weight, hydrodynamic

Table 3. Physico-chemical characteristics of the *F. verticillioides* exopolysaccharide.

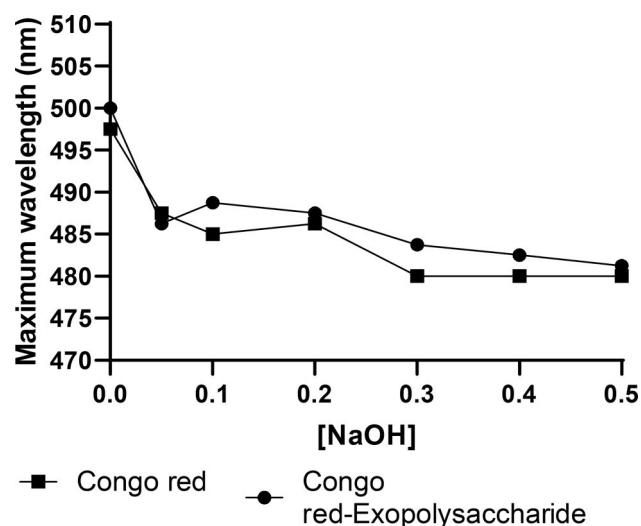| Intrinsic viscosity ([η]) (dl/g)	Viscosity average molar mass (kDa)	Xav hydrodynamic diameter (nm)	Water solubility	Electrical conductivity (mS/cm)
0.022	0.505	4.19	100%	3.58 ± 0.40

Figure 8. Polysaccharide chain conformation (helix or random coil) determination of the *Fusarium verticillioides* exopolysaccharide by Congo red. Maximum absorption wavelengths (λmax) of Congo red solution and Congo red-exopolysaccharide complex at different NaOH concentrations.

diameter, solubility and conductivity, were determined (Table 3). The exopolysaccharide had a low molecular mass of 0.505 kDa. The size distribution analysis suggested that the average particle diameter of the exopolysaccharide was 4.19 nm with a d90 (the particle size with 90% of particles ≤ d90) of 5.26 nm (Table 3). The polydispersity or distribution (PdI) of the exopolysaccharide was 0.18, showing relative homogeneity of its size. The exopolysaccharide also exhibited conductivity (3.58 mS/cm), possibly due to its charged nature (Table 3).

Conformation of the *Fusarium verticillioides* exopolysaccharide structure

The conformation of polysaccharides in solution can be analysed by observing the shift in the maximum

absorption wavelength (λmax) of Congo red dye in the presence of varying concentrations of NaOH. Triple-helix polysaccharides show a bathochromic shift in their λmax when they form a complex with Congo red (Guo et al. 2021). Therefore, the Congo red assay was used to determine the structural conformation of the *F. verticillioides* exopolysaccharide (Figure 8). At 0.0 − 0.20 M NaOH, λmax for Congo red alone and the exopolysaccharide-Congo red complex exhibited a sharp hypsochromic shift and tended to be stable at higher NaOH concentrations. These results indicated that the exopolysaccharide does not have a triple-helix conformation, but rather has a random coil conformation since triple-helix transitions (>15 nm) were not observed for the exopolysaccharide-Congo red complex compared to Congo red alone (Lee et al. 2010; Guo et al. 2021).

Discussion

Members of the genus *Fusarium* cause economically burdensome and hard-to-control diseases, including cankers, crown rot, head blight, scabs, and wilts. Many of these diseases are strongly linked to biofilm formation (Harding et al. 2010; Harding and Daniels 2017; Motaung et al. 2020), as microbes primarily exist in a biofilm state in their natural environments. However, biofilm formation has been formally described in a few *Fusarium* species including *F. oxysporum* f. sp. *cucumerinum* and *F. graminearum* (Peiqian et al. 2014; Shay et al. 2022). Therefore, for many fungal pathogens of plants, including those belonging to *Fusarium*, it is unclear how biofilms form, let along how they impact infections and disease outcomes.

Ten years ago, Miguel and his colleagues observed what looked like *F. verticillioides* biofilms, in which the mycelium was structured in an extracellular material around the hyphae (Miguel et al. 2015). These researchers also discovered a flocculating substance over the cells or small fibrils of hyphae connecting to one another, like a biofilm. To the best of our knowledge, this was the first time that evidence of a biofilm-like structure for *F. verticillioides* had been reported *in vitro*. In the current study, we addressed this knowledge deficit by describing how *F. verticillioides* forms biofilms under *in vitro* conditions.

Information that describes biofilm colony morphologies in stationary liquid cultures is generally lacking in fungal plant pathogen biofilm studies. Filamentous fungi including *F. graminearum* and *F. circinatum* have recently been described as being able

to form biofilm colonies at the air/liquid interface that grow as pellicle–floating masses of cells that cling to each other and move as a unit (Shay et al. 2022; Ratsoma et al. 2024). In this study, we observed floating masses for *F. verticillioides* that are distinguishable from free-living (planktonic) cells by forming colonies displaying a dense, thin, and cloudy material. These results are consistent with several other studies also reporting similar features of fungal and bacterial biofilms (Trautner and Darouiche 2004; Hurlow and Bowler 2009; Coraça-Huber et al. 2020; Santos et al.).

It was also observed that biofilms in *F. verticillioides* developed most efficiently under stationary conditions, while shear stress from shaking conditions prevented proper biofilm formation. Cells incubated in the stationary conditions without shaking had hyphal cells tangled with EPS that appeared to behave like a matrix binding the hyphae together, and cells cultured under agitated conditions seldom clumped together or not at all. The findings are analogous to those reported by Hawser et al. (Hawser et al. 1998), who demonstrated that, under shaking conditions, only a limited number of cells are observable on the surface of cultures. In contrast, cultures maintained under stationary conditions are characterized by the presence of dense networks of hyphae. This might be due to the severe shaking influencing cell architecture, matrix deposition, and biofilm formation (Soll and Daniels 2016). In *C. albicans*, shaking at a speed of 60 rpm prevents biofilm growth, with biofilms exposed to shear stress being thinner than those exposed to non-shaking conditions (Cavalheiro and Teixeira 2018). Hawser et al. (Hawser et al. 1998) also found that lower agitation speeds result in the production of biofilms with no extracellular matrix only hyphae, while shaking at higher speeds results in a biofilm which consists of a few cells on the surface. In the current study, it was observed that some EPS material was present in planktonic cultures; however, this was not as abundant as in biofilm cells, suggesting that under conditions causing agitation of the fungal cells, the cells struggle to produce the EPS matrix.

In light of the above, our findings align with the biofilm concept previously proposed (Harding et al. 2009; Córdova-Alcántara et al. 2019; Motaung et al. 2020). The biofilms of *F. verticillioides* seem to develop through spore adhesion, microcolony formation, maturation, and dispersion. Although many fungal and bacterial species have recorded comparable developmental stages for biofilm formation, filamentous fungal biofilm formation seems to differ from

strain to strain (Mowat et al. 2009; Ramage et al. 2011, 2012; Peiqian et al. 2014). In contrast to unicellular life forms such as yeast and bacteria, most fungi contain many planktonic forms that can disperse and continue the cycle (e.g. sporangia asexual spores, sexual spores, and hyphal fragments), and these dispersive forms most usually float in the air rather than water (Harding et al. 2009). The dispersal phase of biofilms leads to a substantial number of free-living cells in the form of conidia, but in *F. verticillioides* biofilms these cells appeared to be morphologically distinct from normal microconidial spores initially used as inoculum to initiate biofilm formation (Supplementary Figure 1). This suggests that the dispersed biofilm cells differ from normal microconidia. Similar findings were reported in a study on *Bacillus cereus* where the cells in the biofilm have different cell-surface characteristics than their planktonic counterparts. For example, the structure of a polysaccharide linked to peptidoglycan in *B. cereus* could change during biofilm development. Additionally, Boles et al. (Boles et al. 2004) showed that the short-term development of *P. aeruginosa* in biofilms causes considerable genetic diversity in the resident bacteria. The researchers discovered that genetic diversity creates specialized bacterial subpopulations in biofilms, enhancing their ability to withstand physiological stress. However, similar diversity in fungal biofilms has not been observed and needs further study.

The production of the matrix has a high energetic cost, which may be evolutionary justified given the matrix's structural and physicochemical significance in the growth and operation of the biofilm, without which the beneficial emergent properties of biofilms would not be possible (Flemming et al. 2016). This goes to show that the formation of biofilms is closely linked to the formation of the matrix, the bulk of which is extracellular material (Flemming and Wingender 2010; Flemming et al. 2023). As biofilms grow, metabolic activity and EPS production also increase, suggesting that they may become more resistant to abiotic stress (Motaung et al. 2020). In the current study, it was found that *F. verticillioides* developed biofilms under a range of pH and temperature conditions (optimum pH and temperature of 5 and 25 °C, respectively), and a similar trend was previously reported (Ratsoma et al. 2024). Under field conditions, it has been reported that the optimum temperature for spore development is 27 °C, a temperature at which biofilm development could occur. Evaluation of biofilm formation under different pH conditions showed that biofilms were much more robust in somewhat acidic (pH 4–5). These findings are consistent with other reports (Cornet and Gaillardin 2014) since the pH range for fungal development is fairly broad, ranging from pH 3 to more than pH 8, with the optimum at pH 5.0 assuming nutritional needs are met. The capacity to develop a biofilm under varying physical conditions may provide the fungus with survival benefits in inhospitable environments.

The eDNA of the biofilm EPS matrix, has attracted much attention and is considered an interesting component in the study of biofilms. Many studies have uncovered that eDNA plays many important roles in bacteria such as in biofilm structural maintenance through theaction of DNA binding proteins (Whitchurch et al. 2002; Kavanaugh et al. 2019; Buzzo et al. 2021), antimicrobial resistance (Rajendran et al. 2013; Okshevsky and Meyer 2015), and being a reservoir for the interexchange of genes through natural transformation (Merod and Wuertz 2014). Furthermore, eDNA assumes more unusual roles, including acting as a source of energy and nutrients (e.g. carbon, nitrogen and phosphorus) (Pinchuk et al. 2008; Mulcahy et al. 2010; Ibáñez de Aldecoa et al. 2017), and forming higher-order conformations (e.g. G-quadruplex DNA) that further strengthen the biofilm through extracellular EPS-eDNA networks (Seviour et al. 2021). Given these roles, eDNA is an attractive target for antimicrobial drugs to manage biofilm-related infections. However, only a few studies have explored the existence and function of eDNA in filamentous fungi, with no studies conducted in plant pathogenic fungi. In the current study, it was demonstrated that DNase I has an impact on biofilm stability. In a similar study using *A. fumigatus*, DNase I was effective at all concentrations (0.25, 1, and 4 mg/ml) (Rajendran et al. 2013; 2014), but the maximal effect was observed with 4 mg/ml of DNase I (p value < 0.001) which is similar to the observations in this study. The discovery that eDNA contributes significantly to the biofilm EPS in both bacteria and fungi suggests that this may be a conserved and possibly active microbial biofilm process. Nucleic acids are incorporated early in the development of the EPS matrix in *F. graminearum*, and they similarly appear to function as a scaffold, likely regulating the entire matrix structure of the biofilm (Shay et al. 2022). The findings presented in the current study imply that eDNA plays a significant structural maintenance role during biofilm development in a filamentous plant fungal pathogen and may contribute to the severity of the disease.

The *F. verticillioides* exopolysaccharide had a low molecular mass (0.505 kDa) compared to exopolysaccharides from other fungal species, such as that from *F. solani* SD5 (187 kDa) (Mahapatra and Banerjee 2012) and *Cryptococcus laurentii* AL$_{100}$ (4.2 kDa) (Pavlova et al. 2011). It is worth noting that the majority of exopolysaccharide molecular masses reported in the literature are as weight average molecular mass, from size exclusion chromatography (SEC) data (Mahapatra and Banerjee 2013). and while SEC excels in providing detailed size distributions and absolute molecular weights it requires careful calibrationIn contrast, viscometry offers a quicker and simpler approach but relies on empirical relationships that may introduce uncertainty. Lastly, weight-average molecular weight (Mw), as determined by SEC, emphasizes larger molecules and their contributions to physical properties, while Mv focuses on how polymers behave in solution regarding viscosity. Therefore, Mv may not emphasize larger molecules as strongly, leading to molecular weight values lower than those reported by Mw.

The presence of –NH$_2$ and OH groups in the amino sugars composing the exopolysaccharide appear to be important factors that influence the solubility and conductivity of the exopolysaccharide. It is known that the presence of acetyl groups in amino sugars constituting polysaccharides such as chitin increases intermolecular hydrogen bonding, which stabilizes the structure and prevents water from penetrating and dissolving it, therefore, the protonation of these amino groups enhances the *F. verticillioides* exopolysaccharide's solubility in aqueous solutions, particularly in acidic environments.

The particle diameter of the exopolysaccharide isolated from *F. verticillioides* was significantly larger than that isolated from *F. solani* SD5, which was reported to exhibit a diameter of approximately 1 nm using transmission electron microscopy (TEM) (Mahapatra and Banerjee 2013). Considering that *F.verticillioides* exhibited a significantly lower molecular mass than that from *F. solani* SD5 (0.505 versus 187 kDa), we postulate that the *F. verticillioides* exopolysaccharide may exhibit increased entanglement among polysaccharide chains in solution. This entanglement may affect the viscosity and flow properties of the solution, further influencing how the exopolysaccharides arrange themselves, leading to an underestimation of their size.

The cationic nature of the *F. verticillioides* exopolysaccharide may offer a survival advantage to the fungus as it can bind to eDNA and this interaction has the potential to impact on the virulence of the fungus and protect eDNA within the extracellular matrix from digestion. To support this, the cationic *Pseudomonas aeruginosa* Pel exopolysaccharide was shown to bind to eDNA and it was postulated that this interaction likely impacts current therapies by increasing antimicrobial tolerance and protecting eDNA from digestion (Jennings et al. 2021). The production of exopolysaccharides containing α-1,4–linked acetyl-galactosamine (GalNAc) and GalN have also been confirmed in both *Aspergillus* and non-*Aspergillus* spp., including *Neurospora crassa*, *Penicillium frequentans*, *Paecilomyces* sp., and *Trichosporon asahi*, wherein they have been linked to adherence to surfaces or flocculation (Bamford et al. 2020). The *F. verticillioides* exopolysaccharide characterized in this study was highly de-N-acetylated. De-N-acetylation of biofilm exopolysaccharide has been linked to cell aggregation, surface attachment, exopolysaccharide secretion, and biofilm maturation depending on the organism (Bamford et al. 2020).

Conclusions

In the natural environment, plant stem and leaf surfaces can be sparsely or densely colonized by diverse fungal biofilms and are likely more complex than conditions used in this study. Laboratory-grown biofilms are a simple surface-covering, frequently exhibiting confluent and compact uniformity that is consistent with the original definition of biofilms (Harding et al. 2009; Motaung et al. 2020). Documenting biofilm formation in the natural environment by analysing heavily infected plant tissues and a population of field strains, as opposed to a few ones, is needed to better understand what is happening under field conditions. This would enable the development of novel antibiofilm drugs and treatment alternatives to decrease the prevalence of fungal infections. This study thus establishes a baseline with regards to *F. verticillioides* biofilms, showing its intricate structure and response to the environment factors. The anionic exopolysaccharide of this fungus may aid survival by binding to eDNA. This polymer seems to be essential for biofilm integrity, consistent with analyses conducted in human fungal pathogens. Taken together, *F. verticillioides* ability to form biofilms may give it an ecological edge in its battle to keep its place as a commensal and pathogen of maize. The biofilm might enable this fungus to evade host immunity, withstand antifungal treatment and competition from other microbes. The current study,

together with earlier studies, therefore, will deepen the understanding of the relationship between disease outcomes and biotic interactions in *F. verticillioides*. The artificial conditions in this study's *in vitro* biofilm experiments provide insights into *F. verticillioides'* biofilm formation, but may be less complex from the natural maize environment. The study's findings will help infer complex mechanisms during host colonization, using maize tissue or infection models in the future research.

Disclosure statement

Funding

ORCID

Thabiso E. Motaung 🔵 http://orcid.org/0000-0002-8813-7671

References

Albalasmeh AA, Berhe AA, Ghezzehei TA. 2013. A new method for rapid determination of carbohydrate and total carbon concentrations using UV spectrophotometry. Carbohydr Polym. 97:253–261. doi:10.1016/j.carbpol.2013.04.072.

Bamford NC, Le Mauff F, Van Loon JC, Ostapska H, Snarr BD, Zhang Y, Kitova EN, Klassen JS, Codée JDC, Sheppard DC, et al. 2020. Structural and biochemical characterization of the exopolysaccharide deacetylase Agd3 required for Aspergillus fumigatus biofilm formation. Nat Commun. 11:2450. doi:10.1038/s41467-020-16144-5.

Beil S, Schamberger A, Naumann W, Machill S, Pée K-Hv 2012. Determination of the degree of N-acetylation (DA) of chitin and chitosan in the presence of water by first derivative ATR FTIR spectroscopy. Carbohydr Polym. 87:117–122. doi:10.1016/j.carbpol.2011.07.025.

Bixler GD, Bhushan B. 2012. Biofouling: lessons from nature. Philos Trans A Math Phys Eng Sci. 370:2381–2417. doi:10.1098/rsta.2011.0502.

Boles BR, Thoendel M, Singh PK. 2004. Self-generated diversity produces "insurance effects" in biofilm communities. Proc Natl Acad Sci USA. 101:16630–16635. doi:10.1073/pnas.0407460101.

Bradford MM. 1976. A rapid and sensitive method for the quantitation of microgram quantities of protein utilizing the principle of protein-dye binding. Anal Biochem. 72:248–254. doi:10.1016/0003-2697(76)90527-3.

Bruns S, Seidler M, Albrecht D, Salvenmoser S, Remme N, Hertweck C, Brakhage AA, Kniemeyer O, Müller F-MC. 2010. Functional genomic profiling of Aspergillus fumigatus biofilm reveals enhanced production of the mycotoxin gliotoxin. Proteomics. 10:3097–3107. doi:10.1002/pmic.201000129.

Bryers JD. 2008. Medical biofilms. Biotechnol Bioeng. 100:1–18. doi:10.1002/bit.21838.

Buzzo JR, Devaraj A, Gloag ES, Jurcisek JA, Robledo-Avila F, Kesler T, Wilbanks K, Mashburn-Warren L, Balu S, Wickham J, et al. 2021. Z-form extracellular DNA is a structural component of the bacterial biofilm matrix. Cell. 184:5740–5758.e17. doi:10.1016/j.cell.2021.10.010.

Callow JA, Callow ME. 2011. Trends in the development of environmentally friendly fouling-resistant marine coatings. Nat Commun. 2:244. doi:10.1038/ncomms1251.

Cámara M, Green W, MacPhee CE, Rakowska PD, Raval R, Richardson MC, Slater-Jefferies J, Steventon K, Webb JS. 2022. Economic significance of biofilms: a multidisciplinary and cross-sectoral challenge. NPJ Biofilms Microbiomes. 8:42. doi:10.1038/s41522-022-00306-y.

Cavalheiro M, Teixeira MC. 2018. Candida biofilms: threats, challenges, and promising strategies. Front Med (Lausanne). 5:28. doi:10.3389/fmed.2018.00028.

Coraça-Huber DC, Kreidl L, Steixner S, Hinz M, Dammerer D, Fille M. 2020. Identification and morphological characterization of biofilms formed by strains causing infection in orthopedic implants. Pathogens. 9:649. doi:10.3390/pathogens9080649.

Córdova-Alcántara IM, Venegas-Cortés DL, Martínez-Rivera MÁ, Pérez NO, Rodriguez-Tovar AV. 2019. Biofilm characterization of Fusarium solani keratitis isolate: increased resistance to antifungals and UV light. J Microbiol. 57:485–497. doi:10.1007/s12275-019-8637-2.

Cornet M, Gaillardin C. 2014. pH signaling in human fungal pathogens: a new target for antifungal strategies. Eukaryot Cell. 13:691–691. doi:10.1128/EC.00073-14.

Costa-Orlandi CB, Sardi JCO, Santos CT, Fusco-Almeida AM, Mendes-Giannini MJS. 2014. Fungal biofilms and antifungal resistance: an overview. Med Mycol. 52:2–9. doi:10.3109/13693786.2013.763782.

Cruz CD, Shah S, Tammela P. 2018. Defining conditions for biofilm inhibition and eradication assays for Gram-positive clinical reference strains. BMC Microbiol. 18:173. doi:10.1186/s12866-018-1321-6.

Daub CD, Mabate B, Malgas S, Pletschke BI. 2020. Fucoidan from Ecklonia maxima is a powerful inhibitor of the diabetes-related enzyme, α-glucosidase. Int J Biol Macromol. 151:412–420. doi:10.1016/j.ijbiomac.2020.02.161.

Donlan RM. 2001. Biofilm formation: a clinically relevant microbiological process. Clin Infect Dis. 33:1387–1392. doi:10.1086/322972.

Dorst KM, Widmalm G. 2023. NMR chemical shift prediction and structural elucidation of linker-containing oligo- and polysaccharides using the computer program CASPER. Carbohydr Res. 533:108937. doi:10.1016/j.carres.2023.108937.

Flemming H-C, van Hullebusch ED, Neu TR, Nielsen PH, Seviour T, Stoodley P, Wingender J, Wuertz S. 2023. The biofilm matrix: multitasking in a shared space. Nat Rev Microbiol. 21:70–86. doi:10.1038/s41579-022-00791-0.

Flemming H-C, Wingender J, Szewzyk U, Steinberg P, Rice SA, Kjelleberg S. 2016. Biofilms: an emergent form of bacterial life. Nat Rev Microbiol. 14:563–575. doi:10. 1038/nrmicro.2016.94.

Flemming H-C, Wingender J. 2010. The biofilm matrix. Nat Rev Microbiol. 8:623–633. doi:10.1038/nrmicro2415.

Furevi A, Ruda A, Angles d'Ortoli T, Mobarak H, Ståhle J, Hamark C, Fontana C, Engström O, Apostolica P, Widmalm G. 2022. Complete 1H and 13C NMR chemical shift assignments of mono-to tetrasaccharides as basis for NMR chemical shift predictions of oligo- and polysaccharides using the computer program CASPER. Carbohydr Res. 513:108528. doi:10.1016/j.carres.2022. 108528.

Gai X, Dong H, Wang S, Liu B, Zhang Z, Li X, Gao Z. 2018. Infection cycle of maize stalk rot and ear rot caused by Fusarium verticillioides.Sarrocco S, editor. PLoS ONE. 13: e0201588. doi:10.1371/journal.pone.0201588.

Guo X, Kang J, Xu Z, Guo Q, Zhang L, Ning H, Cui SW. 2021. Triple-helix polysaccharides: formation mechanisms and analytical methods. Carbohydr Polym. 262: 117962. doi:10.1016/j.carbpol.2021.117962.

Harding MW, Daniels GC. 2017. In vitro assessment of biofilm formation by soil- and plant-associated microorganisms. In: Ahmad I, Husain FM, editors. Biofilms in plant and soil health. Chichester, UK: John Wiley & Sons, Ltd; [accessed 2020 May 25]; p. 253–273. doi:10. 1002/9781119246329.ch14.

Harding MW, Marques LLR, Howard RJ, Olson ME. 2009. Can filamentous fungi form biofilms? Trends Microbiol. 17:475–480. doi:10.1016/j.tim.2009.08.007.

Harding MW, Marques LLR, Howard RJ, Olson ME. 2010. Biofilm morphologies of plant pathogenic fungi. AmJPSB. 4:43–47.

Hawser SP, Baillie GS, Douglas LJ. 1998. Production of extracellular matrix by Candida albicans biofilms. J Med Microbiol. 47:253–256. doi:10.1099/00222615-47-3-253.

Hurlow J, Bowler PG. 2009. Clinical experience with wound biofilm and management: a case series. Ostomy Wound Manage. 55:38–49.

Ibáñez de Aldecoa AL, Zafra O, González-Pastor JE. 2017. Mechanisms and regulation of extracellular DNA release and its biological roles in microbial communities. Front Microbiol. 8:1390. doi:10.3389/fmicb.2017.01390.

Jennings LK, Dreifus JE, Reichhardt C, Storek KM, Secor PR, Wozniak DJ, Hisert KB, Parsek MR. 2021. Pseudomonas aeruginosa aggregates in cystic fibrosis sputum produce exopolysaccharides that likely impede current therapies. Cell Rep. 34:108782. [accessed 2025 Jan 24]. doi:10.1016/j.celrep.2021.108782.

Karácsony Z, Molnár N, Szabó D, Bakos-Barczi N, Lovas M, Pálfi X, Váczy KZ. 2024. Biofilm formation by the fungus Phaeomoniella chlamydospora: a causal agent of esca disease of grapevine. Mycol Progress. 23:36. doi:10. 1007/s11557-024-01976-y.

Karygianni L, Ren Z, Koo H, Thurnheer T. 2020. Biofilm matrixome: extracellular components in structured microbial communities. Trends Microbiol. 28:668–681. doi:10.1016/j.tim.2020.03.016.

Kavanaugh JS, Flack CE, Lister J, Ricker EB, Ibberson CB, Jenul C, Moormeier DE, Delmain EA, Bayles KW, Horswill AR. 2019. Identification of extracellular DNA-binding proteins in the biofilm matrix.losick r, editor. mBio. 10:e01137-19. doi:10.1128/mBio.01137-19.

Kumirska J, Czerwicka M, Kaczyński Z, Bychowska A, Brzozowski K, Thöming J, Stepnowski P. 2010. Application of spectroscopic methods for structural analysis of Chitin and Chitosan. Mar Drugs. 8:1567–1636. doi:10.3390/md8051567.

Le Mauff F, Razvi E, Reichhardt C, Sivarajah P, Parsek MR, Howell PL, Sheppard DC. 2022. The Pel polysaccharide is predominantly composed of a dimeric repeat of α-1,4 linked galactosamine and N-acetylgalactosamine. Commun Biol. 5:502. doi:10.1038/s42003-022-03453-2.

Lee JS, Kwon JS, Yun JS, Pahk JW, Shin WC, Lee SY, Hong EK. 2010. Structural characterization of immunostimulating polysaccharide from cultured mycelia of Cordyceps militaris. Carbohydr Polym. 80:1011–1017. doi:10.1016/j.carbpol.2010.01.017.

Leggate J, Allain R, Isaac L, Blais BW. 2006. Microplate fluorescence assay for the quantification of double stranded DNA using SYBR Green I dye. Biotechnol Lett. 28:1587–1594. doi:10.1007/s10529-006-9128-1.

Lindsay D, Von Holy A. 2006. Bacterial biofilms within the clinical setting: what healthcare professionals should know. J Hosp Infect. 64:313–325. doi:10.1016/j.jhin.2006. 06.028.

Liu D, Wei Y, Yao P, Jiang L. 2006. Determination of the degree of acetylation of chitosan by UV spectrophotometry using dual standards. Carbohydr Res. 341:782–785. doi:10.1016/j.carres.2006.01.008.

Mahapatra S, Banerjee D. 2012. Structural elucidation and bioactivity of a novel exopolysaccharide from endophytic Fusarium solani SD5. Carbohydr Polym. 90:683–689. doi: 10.1016/j.carbpol.2012.05.097.

Mahapatra S, Banerjee D. 2013. Fungal exopolysaccharide: production, composition and applications. Microbiol Insights. 6:1–16. MBI.S10957. doi:10.4137/MBI.S10957.

Malgas S, Dyk JSv, Abboo S, Pletschke BI. 2016. The inhibitory effects of various substrate pre-treatment by-products and wash liquors on mannanolytic enzymes. J Mol Catal B: enzym. 123:132–140. doi:10.1016/j.molcatb.2015. 11.014.

Marin S, Ramos AJ, Cano-Sancho G, Sanchis V. 2013. Mycotoxins: occurrence, toxicology, and exposure assessment. Food Chem Toxicol. 60:218–237. doi:10.1016/j.fct. 2013.07.047.

Martins M, Henriques M, Lopez-Ribot JL, Oliveira R. 2012. Addition of DNase improves the in vitro activity of antifungal drugs against Candida albicans biofilms. Mycoses. 55:80–85. doi:10.1111/j.1439-0507.2010.01985.x.

Mello TP, Aor AC, Gonçalves DS, Seabra SH, Branquinha MH, Santos ALS. 2016. Assessment of biofilm formation by Scedosporium apiospermum, S. aurantiacum, S. minutisporum and Lomentospora prolificans. Biofouling. 32: 737–749. doi:10.1080/08927014.2016.1192610.

Melo KFS, Rocha LO, Bittencourt LMC, et al. 2022. Fusarium verticillioides biofilm formation relies on a complex extracellular matrix composed of DNA, proteins, and polysaccharides. fJournal of Fungi. 8:824. doi: 10.3390/jof8080824.

Merod RT, Wuertz S. 2014. Extracellular polymeric substance architecture influences natural genetic transformation of acinetobacter baylyi in Biofilms.Spormann AM,

editor. Appl Environ Microbiol. 80:7752–7757. doi:10.1128/AEM.01984-14.

Metcalf D, Bowler P. 2013. Biofilm delays wound healing: a review of the evidence. Burns Trauma. 1:5–12. doi:10.4103/2321-3868.113329.

Miguel TdÁ, Bordini JG, Saito GH, Andrade CGTdJ, Ono MA, Hirooka EY, Vizoni É, Ono EYS. 2015. Effect of fungicide on Fusarium verticillioides mycelial morphology and fumonisin B1 production. Braz J Microbiol. 46:293–299. doi:10.1590/S1517-838246120120383.

Motaung TE, Peremore C, Wingfield B, Steenkamp E. 2020. Plant-associated fungal biofilms—knowns and unknowns. FEMS Microbiol Ecol. 96:fiaa224. doi:10.1093/femsec/fiaa224.

Mowat E, Williams C, Jones B, Mcchlery S, Ramage G. 2009. The characteristics of Aspergillus fumigatus mycetoma development: is this a biofilm? Med Mycol. 47(s1): S120–S126. doi:10.1080/13693780802238834.

Mulcahy H, Charron-Mazenod L, Lewenza S. 2010. Pseudomonas aeruginosa produces an extracellular deoxyribonuclease that is required for utilization of DNA as a nutrient source. Environ Microbiol. 12:1621–1629. [accessed 2022 Sep 1]. doi:10.1111/j.1462-2920.2010.02208.x.

Munkvold GP, Desjardins AE. 1997. Fumonisins in Maize: can We Reduce Their Occurrence? Plant Dis. 81:556–565. doi:10.1094/PDIS.1997.81.6.556.

Okshevsky M, Meyer RL. 2015. The role of extracellular DNA in the establishment, maintenance and perpetuation of bacterial biofilms. Crit Rev Microbiol. 41:341–352. doi:10.3109/1040841X.2013.841639.

Oren L, Ezrati S, Cohen D, Sharon A. 2003. Early events in the fusarium verticillioides-maize interaction characterized by using a green fluorescent protein-expressing transgenic isolate. Appl Environ Microbiol. 69:1695–1701. doi:10.1128/AEM.69.3.1695-1701.2003.

Pavlova K, Rusinova-Videva S, Kuncheva M, Kratchanova M, Gocheva M, Dimitrova S. 2011. Synthesis and characterization of an exopolysaccharide by antarctic yeast strain cryptococcus laurentii AL100. Appl Biochem Biotechnol. 163:1038–1052. doi:10.1007/s12010-010-9107-9.

Peiqian L, Xiaoming P, Huifang S, Jingxin Z, Ning H, Birun L. 2014. Biofilm formation by Fusarium oxysporum f. sp. cucumerinum and susceptibility to environmental stress. FEMS Microbiol Lett. 350:138–145. doi:10.1111/1574-6968.12310.

Pereira AGB, Muniz EC, Hsieh Y-L. 2015. 1H NMR and 1H–13C HSQC surface characterization of chitosan–chitin sheath-core nanowhiskers. Carbohydr Polym. 123:46–52. doi:10.1016/j.carbpol.2015.01.017.

Pinchuk GE, Ammons C, Culley DE, Li S-MW, McLean JS, Romine MF, Nealson KH, Fredrickson JK, Beliaev AS. 2008. Utilization of DNA as a sole source of phosphorus, carbon, and energy by Shewanella spp.: ecological and physiological implications for dissimilatory metal reduction. Appl Environ Microbiol. 74:1198–1208. doi:10.1128/AEM.02026-07.

Prashanth KVH, Kittur FS, Tharanathan RN. 2002. Solid state structure of chitosan prepared under different N-deacetylating conditions. Carbohydr Polym. 50:27–33. doi:10.1016/S0144-8617(01)00371-X.

Rajendran R, Sherry L, Lappin DF, Nile CJ, Smith K, Williams C, Munro CA, Ramage G. 2014. Extracellular

DNA release confers heterogeneity in Candida albicans biofilm formation. BMC Microbiol. 14:303. doi:10.1186/s12866-014-0303-6.

Rajendran R, Williams C, Lappin DF, Millington O, Martins M, Ramage G. 2013. Extracellular DNA release acts as an antifungal resistance mechanism in mature aspergillus fumigatus biofilms. Eukaryot Cell. 12:420–429. doi:10.1128/EC.00287-12.

Ramage G, Rajendran R, Gutierrez-Correa M, Jones B, Williams C. 2011. Aspergillus biofilms: clinical and industrial significance. FEMS Microbiol Lett. 324:89–97. doi:10.1111/j.1574-6968.2011.02381.x.

Ramage G, Rajendran R, Sherry L, Williams C. 2012. Fungal biofilm resistance. Int J Microbiol. 2012: 1–14. doi:10.1155/2012/528521.

Ratsoma FM, Mokoena NZ, Santana QC, Wingfield BD, Steenkamp ET, Motaung TE. 2024. Characterization of the Fusarium circinatum biofilm environmental response role. J Basic Microbiol. 64:e2300536. doi:10.1002/jobm.202300536.

Seviour T, Winnerdy FR, Wong LL, Shi X, Mugunthan S, Foo YH, Castaing R, Adav SS, Subramoni S, Kohli GS, et al. 2021. The biofilm matrix scaffold of Pseudomonas aeruginosa contains G-quadruplex extracellular DNA structures. NPJ Biofilms Microbiomes. 7:27. doi:10.1038/s41522-021-00197-5.

Shashkov AS, Paramonov NA, Veremeychenko SP, Grosskurth H, Zdorovenko GM, Knirel YA, Kochetkov NK. 1998. Somatic antigens of pseudomonads: structure of the O-specific polysaccharide of Pseudomonas fluorescens biovar B, strain IMV 247. Carbohydr Res. 306:297–303. doi:10.1016/S0008-6215(97)10048-9.

Shay R, Wiegand AA, Trail F. 2022. Biofilm formation and structure in the filamentous fungus fusarium graminearum, a Plant Pathogen.Wang Y, editor. Microbiol Spectr. 10:e00171–22. doi:10.1128/spectrum.00171-22.

Soll DR, Daniels KJ. 2016. Plasticity of Candida albicans biofilms. Microbiol Mol Biol Rev. 80:565–595. doi:10.1128/MMBR.00068-15.

Song M, Wang J, Bao K, Sun C, Cheng X, Li T, Wang S, Wang S, Wen T, Zhu Z. 2024. Isolation, structural characterization and immunomodulatory activity on RAW264.7 cells of a novel exopolysaccharide of Dictyophora rubrovalvata. Int J Biol Macromol. 270: 132222. doi:10.1016/j.ijbiomac.2024.132222.

Torres PB, Nagai A, Jara CEP, Santos JP, Chow F, Santos D. 2021. Determination of sulfate in algal polysaccharide samples: a step-by-step protocol using microplate reader. Ocean Coast Res. 69:e21021. doi:10.1590/2675-2824069.21-010pbt.

Trabelsi L, M'sakni NH, Ben Ouada H, Bacha H, Roudesli S. 2009. Partial characterization of extracellular polysaccharides produced by cyanobacterium Arthrospira platensis. Biotechnol Bioproc E. 14:27–31. doi:10.1007/s12257-008-0102-8.

Trautner BW, Darouiche RO. 2004. Role of biofilm in catheter-associated urinary tract infection. Am J Infect Control. 32:177–183. doi:10.1016/j.ajic.2003.08.005.

Turska-Szewczuk A, Duda K, Schwudke D, Pekala A, Kozinska A, Holst O. 2014. Correction: structural studies of the lipopolysaccharide from the fish pathogen aeromonas veronii strain Bs19, Serotype O16. Mar. Drugs 2014,

12, 1298–1316. Mar Drugs. 12:4741–4742. doi:10.3390/md12094741.

Vårum KM, Anthonsen MW, Grasdalen H, Smidsrød O. 1991. Determination of the degree of N-acetylation and the distribution of N-acetyl groups in partially N-deacetylated chitins (chitosans) by high-field n.m.r. spectroscopy. Carbohydr Res. 211: 17–23. doi:10.1016/0008-6215(91)84142-2.

Vinogradov E, Perry MB. 2004. Characterisation of the core part of the lipopolysaccharide O-antigen of Francisella novicida (U112). Carbohydr Res. 339:1643–1648. doi:10.1016/j.carres.2004.04.013.

Whitchurch CB, Tolker-Nielsen T, Ragas PC, Mattick JS. 2002. Extracellular DNA required for bacterial biofilm formation. Science. 295:1487–1487. doi:10.1126/science.295.5559.1487.

Wild CP, Gong YY. 2010. Mycotoxins and human disease: a largely ignored global health issue. Carcinogenesis. 31: 71–82. doi:10.1093/carcin/bgp264.

Wu T, Zivanovic S. 2008. Determination of the degree of acetylation (DA) of chitin and chitosan by an improved first derivative UV method. Carbohydr Polym. 73:248–253. doi:10.1016/j.carbpol.2007.11.024.